



POLITECNICO
MILANO 1863

SCUOLA DI INGEGNERIA INDUSTRIALE
E DELL'INFORMAZIONE

EXECUTIVE SUMMARY OF THE THESIS

A Trefftz Discontinuous Galerkin method with Absorbing Boundary Conditions for the numerical simulation of the Helmholtz problem

LAUREA MAGISTRALE IN MATHEMATICAL ENGINEERING - INGEGNERIA MATEMATICA

Author: SIMONE PESCUMA

Advisor: PROF.SSA PAOLA F. ANTONIETTI

Co-advisors: DR. AXEL MODAVE, PROF. GWÉNAËL GABARD

Academic year: 2021-2022

1. Introduction

In acoustics, the propagation phenomenon is modeled by the wave equation, that reduces to the Helmholtz equation in the frequency domain. In this framework, standard Finite Element Methods with linear basis functions suffer from the numerical pollution effect which deteriorates the numerical solution. Several approaches have been studied to deal with it. The two main classes of methods include: local high-order polynomial methods and Trefftz methods. We focus on Trefftz methods with wave-based basis functions and more specific on the Ultra Weak Variational Formulation (UWVF). They rely on the largely accepted intuition that the use of shape functions that are local solutions of Helmholtz equation allows to incorporate physical characteristics of the problem and to require a number of degrees of freedom that is smaller than that required by polynomial methods ([1]). Although most of wave propagation problems are defined in the whole space, namely an unbounded domain, numerical solutions computed with finite elements demand computational domains that are as small as possible. Hence, they are retrieved with modified problems defined on truncated domains with artificial boundaries.

Even though the latter are not physical, these boundaries must be carefully modeled in order to recover the solution corresponding to the original physical problems. Hence, finite element methods must be coupled with domain truncation techniques, which simulate the outward propagation of waves at the boundary of the computational domain ([2, 3]), for example by imposing Absorbing Boundary Conditions (ABCs) in such a way that all outgoing waves are allowed to pass the artificial boundary unaffected, in particular without being reflected, while no incoming wave is allowed into the domain from outside.

In this thesis, we focus on the coupling of the UWVF with ABCs and, in particular, we study its continuous and high-order formulation. The latter represents a novelty that, to the best of our knowledge, has never been studied before. Therefore, the goal of this work is to investigate the behaviour of numerical solutions obtained in this new framework in order to study the efficiency of the method.

After introducing the model (Sec. 2), we describe the UWVF with ABCs (Sec. 3), its discretization (Sec. 4) and conclude by presenting some numerical results (Sec. 5).

2. Helmholtz problem

Let $\Omega \subset \mathbb{R}^2$ be a domain as shown in Fig. 1. For $u : \Omega \rightarrow \mathbb{C}$ with an implicit time dependence $e^{-i\omega t}$, where ω is the angular frequency and i is the imaginary unit, we consider the following boundary-value model problem set in terms of Helmholtz equation

$$\begin{cases} \Delta u + \kappa^2 u = 0, & \mathbf{x} \in \Omega, \\ \partial_{\mathbf{n}} u = \mathcal{B}u, & \mathbf{x} \in \Gamma_{\text{ext}}, \\ \partial_{\mathbf{n}} u = g, & \mathbf{x} \in \Gamma_{\text{int}}, \end{cases} \quad (1)$$

where $\kappa = \omega/c$ is the wavenumber, c is the speed of sound, Γ_{ext} and Γ_{int} are the external and internal boundary of Ω , respectively, \mathbf{n} is the outward unit normal on $\partial\Omega$ and \mathcal{B} is a suitable operator that permits to model absorption on Γ_{ext} .

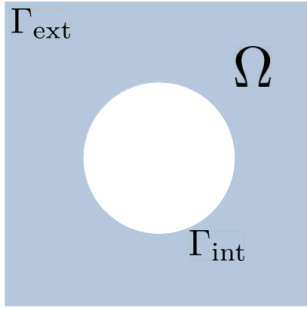


Figure 1: Example of truncated domain Ω with artificial boundary Γ_{ext} .

We review three kinds of ABCs. In [2], the exact absorbing boundary condition is derived in the case of straight boundary. In particular, the pseudo-differential operator \mathcal{B} that appears in (1) is written in terms of the Laplace–Beltrami operator Δ_{Γ} as follows

$$\mathcal{B} \equiv \mathcal{B}_{\text{sqrt}} = i\kappa \sqrt{1 + \Delta_{\Gamma}/\kappa^2}, \quad \Delta_{\Gamma} = \Delta - \partial_{\mathbf{nn}}. \quad (2)$$

Besides its explicit form, it is possible to approximate the square root in (2) in order to derive High-Order Absorbing Boundary Conditions (HABCs). A family of HABCs was introduced in [2] by using the Padé approximation of the square root. In particular, the $(2N + 1)$ th-order Padé approximation of the square root (with a rotation of the branch cut by an angle ϕ) leads to the condition

$$\partial_{\mathbf{n}} u = \mathcal{B}_{\text{Padé}} u, \quad \mathbf{x} \in \Gamma_{\text{ext}},$$

with the pseudo-differential operator $\mathcal{B}_{\text{Padé}}$ defined as

$$\mathcal{B}_{\text{Padé}} = i\kappa e^{i\phi/2} \left[1 + \frac{2}{M} \sum_{n=1}^N c_n \left(1 - \frac{e^{i\phi}(c_n + 1)}{(e^{i\phi} c_n + 1) + \Delta_{\Gamma}/\kappa^2} \right) \right],$$

with $c_n = \tan^2(n\pi/M)$ and $M = 2N + 1$.

Taking $N = 0$ and $\phi = 0$, we get the lowest-order boundary condition

$$\partial_{\mathbf{n}} u = \mathcal{B}_{i\kappa} u, \quad \mathbf{x} \in \Gamma_{\text{ext}},$$

with $\mathcal{B}_{i\kappa} = i\kappa$.

3. UWVF with ABCs

Considering a non-overlapping triangulation \mathcal{T}_h composed of K elements T_i with $i = 1, \dots, K$, we take the space of solutions

$$V = \prod_{i=1}^K \{v_i \in H^1(T_i) : \Delta v_i + \kappa^2 v_i = 0\}. \quad (3)$$

To build the approximation space, we consider a set of P plane waves as basis functions for each element.

To be the solution of problem (1), a field $u \in V$ must satisfy compatibility conditions on each interface. For a given interface $\bar{F}_{ij} = \partial T_i \cap \partial T_j$, where T_i and T_j are two neighboring elements (Fig. 2), they read

$$u_i = u_j, \quad \mathbf{x} \in F_{ij}, \quad (4)$$

$$\partial_{\mathbf{n}_i} u_i + \partial_{\mathbf{n}_j} u_j = 0, \quad \mathbf{x} \in F_{ij}, \quad (5)$$

where \mathbf{n}_i is the outward unit normal on ∂T_i and u_i is the restriction of u on T_i . Notice that the previous conditions guarantee the continuity of the acoustic pressure and normal particle velocity, respectively, across the element interfaces.

The matching conditions on the interfaces and the boundary conditions can be written in terms of proper outgoing and incoming traces. For the boundary ∂T_i of any element $T_i \in \mathcal{T}$, we introduce the outgoing operator \mathcal{O}_i and incoming operator \mathcal{I}_i defined as

$$\mathcal{O}_i = \frac{1}{2} \left(\frac{1}{i\kappa} \frac{\partial}{\partial \mathbf{n}_i} + 1 \right), \quad \mathcal{I}_i = \frac{1}{2} \left(-\frac{1}{i\kappa} \frac{\partial}{\partial \mathbf{n}_i} + 1 \right). \quad (6)$$

The applications of \mathcal{O}_i and \mathcal{I}_i on u_i can be considered approximations of the outgoing and incoming fields, respectively.

The matching conditions (4) and (5) can be equivalently written as

$$\mathcal{O}_i u_i = \mathcal{O}_i u_j, \quad \mathcal{O}_j u_i = \mathcal{O}_j u_j.$$

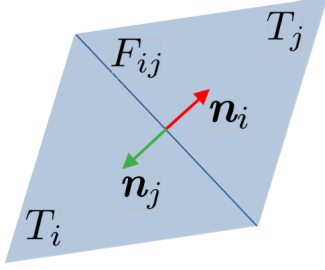


Figure 2: Notation regarding two adjacent triangular elements $T_i, T_j \in \mathcal{T}$.

Taking into account the Helmholtz equation appearing in (1) and (3), multiplying both sides of the equations by the conjugate of v , that is \bar{v} , and u , respectively, integrating by parts and exploiting the definitions of outgoing and incoming traces (6), it is possible to derive the UWVF of the problem, that is given in the following theorem.

Theorem 3.1. *If the solution $u \in H^1(\Omega)$ of problem (1) is regular enough in Ω (that is all its required derivatives are in $L^2(\partial T_i)$ for any $i = 1, \dots, K$), then u satisfies*

$$\begin{aligned} & \sum_i \int_{\partial T_i} \mathcal{O}_i u_i \overline{\mathcal{O}_i v_i} - \sum_i \int_{\Gamma_i^{ext}} -\frac{1}{2i\kappa} \mathcal{B} u_i \overline{\mathcal{I}_i v_i} \\ & - \sum_i \sum_{j \neq i} \int_{F_{ij}} \mathcal{O}_j u_j \overline{\mathcal{I}_i v_i} - \sum_i \int_{\Gamma_i} \frac{1}{2} u_i \overline{\mathcal{I}_i v_i} \\ & = \sum_i \int_{\Gamma_i^{int}} -\frac{1}{2i\kappa} g \overline{\mathcal{I}_i v_i} \end{aligned} \quad (7)$$

for all $v \in V$.

This formulation is an extension of the one presented in [4], indeed we consider a more general ABC operator \mathcal{B} with respect to the one taken into account in [4], which is $\mathcal{B} = i\kappa$.

4. Plane-wave discretization

We apply the Galerkin wave-based method considering a plane-wave basis, that is

$$\{v_p\}_{1 \leq p \leq P}, \quad v_p(\mathbf{x}) = \exp(i\kappa \mathbf{d}_p \cdot \mathbf{x}), \quad (8)$$

where \mathbf{d}_p with $p = 1, \dots, P$ belongs to a finite subset

$$\mathbb{S}_2^P = \{\mathbf{d}_1, \dots, \mathbf{d}_P\},$$

consisting of P different directions of the unit circle \mathbb{S}_2 of \mathbb{R}^2 and \mathbf{x} is a generic point of the plane. The parameter P refers to the number of plane waves used in each $T_i \in \mathcal{T}_h$.

Using this basis, the solution in T_i has the following discretized form

$$u_i^P = \sum_{p=1}^P \alpha_{i,p} v_p, \quad (9)$$

where $\alpha_{i,p} \in \mathbb{C}$ are the coefficients of the linear combination of the plane-wave basis elements. On each element $T_i \in \mathcal{T}_h$ we can define a different set of shape functions, which means that P may depend on the element, as well as the distribution of the directions over \mathbb{S}_2 . This remark lets directional adaptivity possible for the present method.

Finally, for the moment, we consider a system of directions for the plane-wave basis uniformly distributed over \mathbb{S}_2 , *i.e.*

$$\mathbf{d}_p = (\cos \theta_p, \sin \theta_p),$$

$$\theta_p = \theta_1 + (p-1)(2\pi/P), \quad p = 1, \dots, P.$$

The first angle θ_1 is called *shift*. An example is shown in Fig. 3.

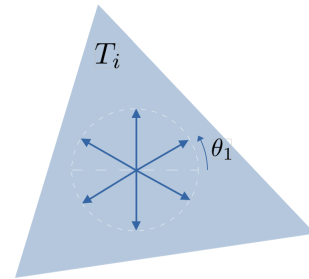


Figure 3: Example of $P = 6$ uniformly spaced directions, with $\theta_1 = \pi/6$.

The use of the numerical solution (9) and the plane waves (8) as test functions in formulation (7) leads to a linear system whose unknown vector corresponds to the coefficients $\alpha_{i,p}$. In order to give an explicit form to the matrix and the right hand side vector, we consider their blocks related to an element T_i and summing on all the elements we get the final result. Taking into account each integral that appears in (7), we can rewrite it in terms of plane wave discretization using (9).

Each outgoing $\mathcal{O}_i u_i$ and incoming trace $\mathcal{I}_i u_i$ can be written as

$$\mathcal{O}_i u_i^P = \sum_{p=1}^P \alpha_{i,p} \frac{1}{2} \left(\frac{1}{i\kappa} \partial_{\mathbf{n}_i} v_p + v_p \right),$$

$$\mathcal{I}_i u_i^P = \sum_{p=1}^P \alpha_{i,p} \frac{1}{2} \left(-\frac{1}{i\kappa} \partial_{\mathbf{n}_i} v_p + v_p \right).$$

Substituting the previous discrete expressions of the outgoing and incoming traces into (7), we are able to retrieve the matrix form of the discretized problem as the following proposition claims

Proposition 4.1. *Formulation (7) is associated to the following algebraic linear system*

$$(M - E)\alpha = c,$$

where the matrices M , $E = E_1 + E_2 + E_3$ and the vector c read

$$\begin{aligned} M_{ii,pq} &= \Lambda_{i,q}^+ \Lambda_{i,p}^+ \int_{\partial T_i} v_p \bar{v}_q ds, \\ E_{1,ij,pq} &= \Lambda_{i,q}^- \Lambda_{j,p}^+ \int_{F_{ij}} v_p \bar{v}_q ds, \\ E_{2,ii,pq} &= -\frac{1}{2i\kappa} \Lambda_{i,q}^- \int_{\Gamma_i^{ext}} \mathcal{B} v_p \bar{v}_q ds, \\ E_{3,ii,pq} &= \frac{1}{2} \Lambda_{i,q}^- \int_{\Gamma_i} v_p \bar{v}_q ds, \\ c_{i,q} &= -\frac{1}{2i\kappa} \Lambda_{i,q}^- \int_{\Gamma_i^{int}} g \bar{v}_q ds, \end{aligned}$$

where $\Lambda_{i,p}^\pm = \frac{1}{2}(1 \pm \mathbf{d}_p \cdot \mathbf{n}_i)$, the indexes $i, j = 1, \dots, K$ identify the block related to the boundary of an element T_i or the face shared by two elements T_i, T_j and the indexes $p, q = 1, \dots, P$ identify one of its elements.

5. Numerical results

We briefly present the main results regarding the two most important numerical experiments that have been carried out.

5.1. Case with one square element

Let $\Omega = (0, 1) \times (0, 1)$ be a domain. We consider the following model boundary-value problem set in terms of Helmholtz equation for $u : \Omega \rightarrow \mathbb{C}$

$$\begin{cases} \Delta u + \kappa^2 u = 0, & \mathbf{x} \in \Omega, \\ \partial_{\mathbf{n}} u = \mathcal{B}u, & \mathbf{x} \in \Gamma^{ABC}, \\ \partial_{\mathbf{n}} u = \partial_{\mathbf{n}} u^{\text{ref}}, & \mathbf{x} \in \Gamma^N. \end{cases}$$

where Γ^{ABC} stands for the portion of boundary of Ω where ABCs are applied, Γ^N for its complementary where Neumann boundary conditions are applied, so that $\partial\Omega = \Gamma^{ABC} \cup \Gamma^N$. The exact solution reads $u^{\text{ref}}(\mathbf{x}) = e^{i\kappa(\hat{\mathbf{d}} \cdot \mathbf{x})}$, $\hat{\mathbf{d}} = (\cos \alpha, \sin \alpha)^T$, $\alpha \in [0, 2\pi]$ and it is shown in Fig. 4.

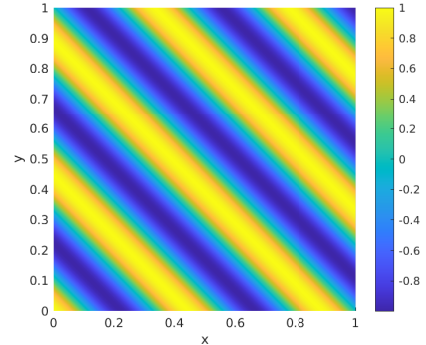


Figure 4: Real part of the exact solution u^{ref} ($\alpha = \pi/4$, $\kappa = 20$).

We consider two settings that we denote ‘case 1’ and ‘case 2’ as displayed below in Fig. 5.

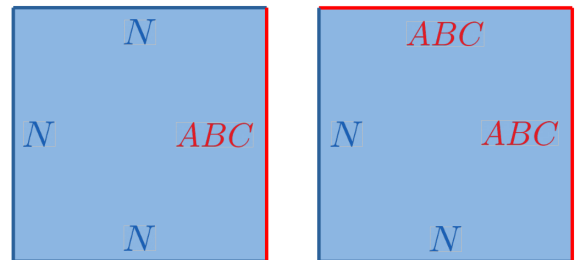


Figure 5: Case 1 (left) and case 2 (right).

We consider a single numerical element and show in Fig. 6 and Fig. 7 the L^2 -error plots with respect to the number P of basis functions uniformly distributed in the quarter $[0, \pi/2]$.

The case with $\mathcal{B}_{l\kappa}$ is the one that presents the largest error, since it incorporates the source of error associated to the approximate model of the ABC. The case with $\mathcal{B}_{\text{sqrt}}$ has a smaller error and close to the Neumann case since the ABC is exact. We can observe that increasing the order of the Padé approximation, we are able to retrieve an increasingly smaller error until a certain threshold, that is the one established by the error obtained in the case with $\mathcal{B}_{\text{sqrt}}$. Once the sqrt-threshold is achieved, it is no longer possible to decrease the error, indeed Padé approximates the exact formulation of the ABC given by $\mathcal{B}_{\text{sqrt}}$. Increasing too much the number P of basis functions leads to conditioning issues ([5]) and unreliable results. Finally, a first investigation regarding the error plots shows no evident particular anomaly in the corner areas, contrary to polynomial methods ([3]) that require a specific corner treatment.

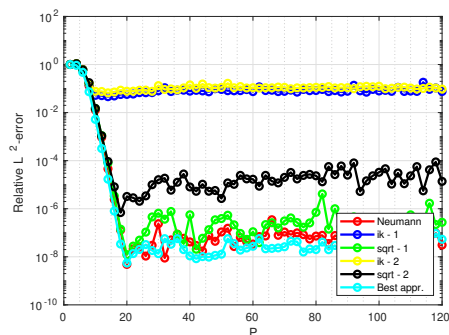


Figure 6: Relative L^2 -error w.r.t. P with $\alpha = \frac{\pi}{4}$, $\kappa = 20$ and several types of B.C.

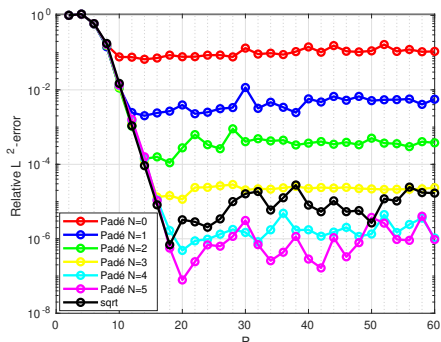


Figure 7: Relative L^2 -error w.r.t. P with $\alpha = \frac{\pi}{4}$, $\kappa = 20$ and several types of B.C. (case 2).

5.2. Case with unstructured mesh

Let $\Omega = \Omega_{\text{square}} \setminus \Omega_{\text{circle}} = (-1.2, 1.2) \times (-1.2, 1.2) \setminus \{(x, y) \in \mathbb{R}^2 : x^2 + y^2 \leq 1\}$. We consider the scattering of the incident plane wave $u^{\text{inc}}(\mathbf{x}) = e^{i\kappa \mathbf{k} \cdot \mathbf{x}}$, where \mathbf{k} is its direction, by the circular cylinder of unit radius centered at the origin generates a scattered field u^{ref} which can be explicit expressed in a closed form by polar coordinates. It is shown in Fig. 8. We consider the following (sound-hard) scattering problem for $u : \Omega \rightarrow \mathbb{C}$

$$\begin{cases} \Delta u + \kappa^2 u = 0, & \mathbf{x} \in \Omega, \\ \partial_{\mathbf{n}} u = \mathcal{B}u, & \mathbf{x} \in \Gamma_{\text{ext}}, \\ \partial_{\mathbf{n}} u = -\partial_{\mathbf{n}} u^{\text{inc}}, & \mathbf{x} \in \Gamma_{\text{int}}. \end{cases}$$

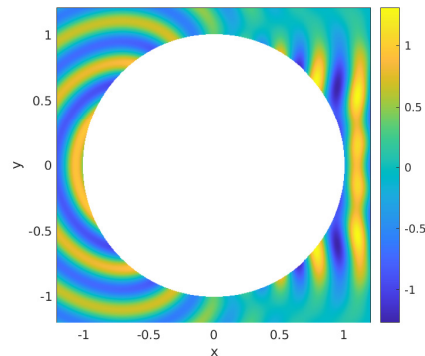


Figure 8: Real part of the exact solution u^{ref} with $\mathbf{k} = (1, 0)$ and $\kappa = 20$.

The numerical simulations have been performed by using an unstructured mesh. We show in Fig. 9, Fig. 10, Fig. 11. and Fig. 12 the L^2 -error plots in both case of h and P refinements. The considerations regarding the cases with $\mathcal{B}_{l\kappa}$ and $\mathcal{B}_{\text{sqrt}}$, as well as the conditioning, are still valid. A problem concerning Padé approximation arises. Indeed, we expect the error to decrease in a significant way increasing the order of the approximation N . It may be caused by a combination of different sources of error:

- Modeling error: no corner treatment has been taken into account.
- Conditioning: it leads to the deterioration of the numerical solution.
- Numerical error: related to the numerical scheme we use.

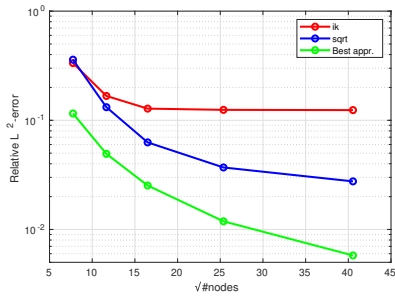


Figure 9: Relative L^2 -error w.r.t $\sqrt{\#\text{nodes}}$ with $\mathbf{k} = (1, 0)$, $\kappa = 20$, $P = 8$ and several types of B.C.

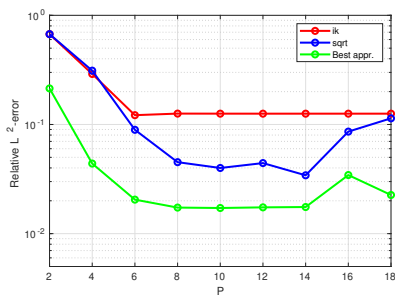


Figure 10: Relative L^2 -error w.r.t P with $\mathbf{k} = (1, 0)$, $\kappa = 20$, $h = 0.1$ and several types of B.C.

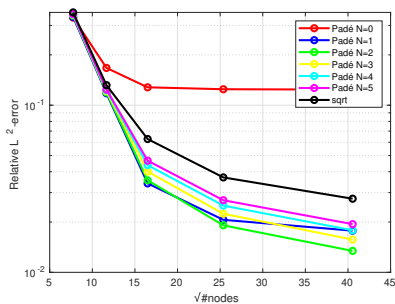


Figure 11: Relative L^2 -error w.r.t $\sqrt{\#\text{nodes}}$ with $\mathbf{k} = (1, 0)$, $\kappa = 20$, $P = 8$ and several types of B.C.

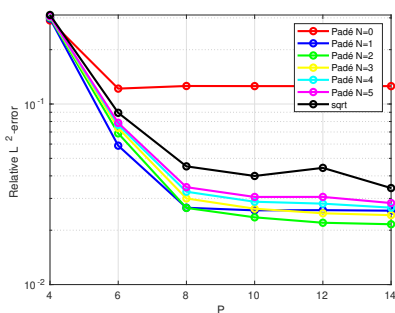


Figure 12: Relative L^2 -error w.r.t P with $\mathbf{k} = (1, 0)$, $\kappa = 20$, $h = 0.1$ and several types of B.C.

6. Conclusions

We have investigated the combination of the Ultra Weak Variational Formulation with Absorbing Boundary Conditions in the framework of a Trefftz method applied to Helmholtz equation. In particular, we have extended the formulation derived in [4] and we have implemented a finite element solver to perform numerical simulations. The simulations show a better behaviour of the absorbing boundary condition based on $\mathcal{B}_{\text{sqrt}}$ rather than its zeroth-order approximation \mathcal{B}_{ik} . Moreover, the use of Padé approximation $\mathcal{B}_{\text{Padé}}$ presents some issues and unexpected effects. However, we can confirm its converging behaviour to the exact formulation given by the operator $\mathcal{B}_{\text{sqrt}}$ with respect to the order N of the Padé approximation.

Acknowledgments

This work was supported in part by the ANR JCJC project WavesDG (research grant ANR-15-CE23-0017-01).

References

- [1] A. Lieu, G. Gabard, H. Bériot, *A comparison of high-order polynomial and wave-based methods for Helmholtz problems*, J. Comput. Phys. 321 (2016) 105-125
- [2] B. Engquist, A. Majda, *Absorbing boundary conditions for numerical simulation of waves*, Proc. Natl. Acad. Sci. 74 (1977) 1765-1766
- [3] A. Modave, C. Geuzaine, X. Antoine, *Corner treatments for high-order local absorbing boundary conditions in high-frequency acoustic scattering*, J. Comput. Phys. 401 (2020)
- [4] O. Cessenat, B. Després, *Application of an ultra weak variational formulation of elliptic PDEs to the two-dimensional Helmholtz problem*, J. Comput. Phys. 35 (1998)
- [5] H. Barucq, A. Bendali, J. Diaz, S. Tordeux, *Local strategies for improving the conditioning of the plane-wave ultra-weak variational formulation*, J. Comput. Phys. 441 (2021)